Chapter 2
Effects of Magneto-Mechanical Coupling on Structural Modal Parameters

M. Kirschneck, D.J. Rixen, Henk Polinder, and Ron van Ostayen

Abstract Structures that are exposed to a magnetic field experience magnetic forces. As these forces are geometry dependent they vary with the displacement of the structure that can result in an additional stiffness. Furthermore eddy currents induced by the movement of the structure can lead to an increased dissipation resulting in a higher damping value for the mechanical part of the system. This paper introduces calculation techniques for predicting these effects and validates them with measurements done on a simple set up in the lab.

Keywords Modal parameter identification • Magneto-mechanical coupling • Monolithic eigenvalue problem

2.1 Introduction

All ferro-magnetic objects, that are exposed to a magnetic field, experiences local forces. For an object at rest in a magnetic field these local forces cancel each other out and the net force on the object is zero. But when the magnetic field is such that the local forces do not balance each other out the object experiences a net force. In such a case the magnetic force has an effect on the mechanics of the system. At the same time the change of geometry due to movement will affect the magnetic field. These kind of systems are called two way magneto-mechanically coupled systems. In such as system the dynamical behavior of can be altered compared to its behavior without that coupling. This also has an impact on the modal parameters that the system displays under no coupling conditions. Certain configurations and geometries contribute to the impact of the effect of the magneto-mechanical coupling. In this paper such a system is introduced and it is shown how the change on modal parameters can be simulated and predicted.

There has been extensive research on magneto-mechanical systems. In fact many transducer that transforms electric energy to mechanic energy or the other way around, i.e. electric machines, are magneto-mechanical coupled systems. Therefore the research on magneto-mechanical coupled systems began by the discovery of forces due to electric currents and their mentioning by Maxwell [7].

In light weight structures the opposing aims of making a structure as stiff as possible and as light as possible is commonly found. For these kind of structures that are exposed to magnetic fields, the exact knowledge of the dynamics of the structure might be crucial. The knowledge might allow to reduce the weight of the structure further. The same is true for electric machines that operate in places where weight reduction is essential. The rotors and stators of these machines are exposed to magnetic fields while being required to be as stiff and as light as possible. Applications can be found in electric cars or large off-shore direct-drive wind turbines.

M. Kirschneck (✉) • R. van Ostayen
Faculty of Mechanical, Maritime and Materials Engineering, Delft University of Technology, Stevinweg 1, 2628 CN Delft, The Netherlands
e-mail: m.kirschneck@tudelft.nl

D.J. Rixen
Faculty of Mechanical Engineering, Technical University of Munich, Boltzmannstr. 15, 85748 München, Germany

H. Polinder
Faculty of Electrical Engineering Mathematics and Computer Science, Delft University of Technology, Stevinweg 1, 2628 CN Delft, The Netherlands

R. Allemang (ed.), *Topics in Modal Analysis II, Volume 8: Proceedings of the 32nd IMAC, A Conference and Exposition on Structural Dynamics, 2014*, Conference Proceedings of the Society for Experimental Mechanics Series,
DOI 10.1007/978-3-319-04774-4_2,

Recent research on dynamics of magneto-mechanical coupled system concentrated on one way coupled formulations [4, 8, 9]. The reason for this is that 3D magnetic calculations are expensive and are avoided unless absolutely necessary. Research on 3D two way coupled problems has been done but not applied to modal analysis [2].

2.2 The Test Setup

The test set up consists of a stator yoke, two permanent magnets and a flexible beam. Figure 2.1 shows a photo of the test set up and a 3D schematic of it. The coil that can be seen in the picture was not used for the experiments. The stator yoke is fixed to the table by clamps. The flexible beam is fixed to a table that can be moved. This construction allows to move the front part of the beam in and out of the air gap of the stator yoke. The two permanent magnets are located in the air gap and create the magnetic field that passively interacts with the structural dynamics (Table 2.1). Because neither the stator yoke nor the beam are slotted eddy currents are possible in the system and heat dissipation can occur.

2.2.1 Emerging Effects

The beam is constructed in such a way that the first bending frequency in one direction is much lower than in the other directions. The bending mode shown in Fig. 2.1b will decrease the air gap length on one side of the beam while it is increased on the other side of the beam. This will change the magnetic field in the air gap. Due to fringe effects the magnetic flux density will rise on the side where the air gap length is reduced and diminish where the air gap lengthened. The resulting magnetic force that acts on the beam and pulls the beam in both air gaps towards the yoke will also change. Because the force does not depend linearly on the air gap length but is proportional to $1/l$, where l is the air gap length, the forces will no longer even each other out and the beam will see a force pulling it in the same direction as the displacement. From a dynamical point of view this can be seen as an additional negative stiffness that is introduced into the system when the beam oscillates. As a result the oscillation frequency of the first bending mode will decrease.

Additionally the time changing magnetic field will induce eddy currents in the stator yoke counter acting the change of the magnetic field. The result is that the peak of the magnetic field has a short delay compared to the peak of the displacement.

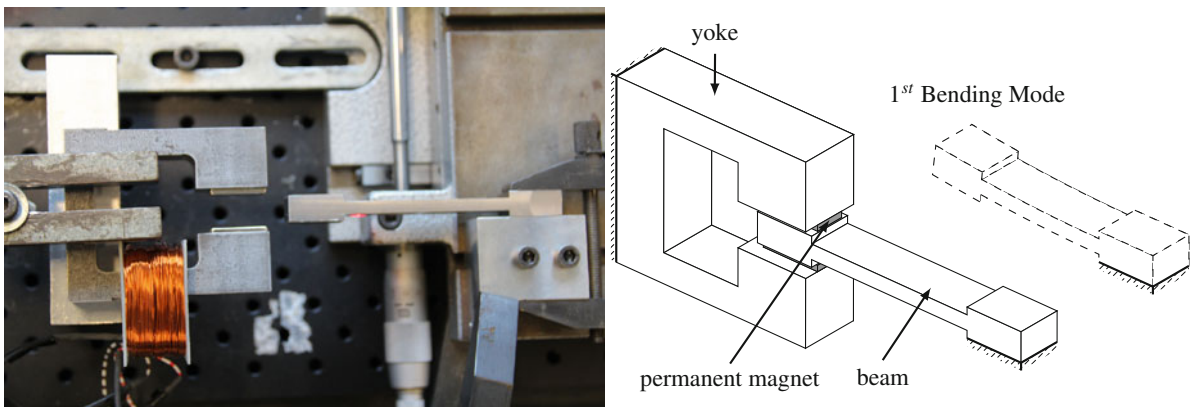

Fig. 2.1 The test rig used for measurements

Table 2.1 Specification of permanent magnets as documented by the suppliers (if documented)

Property	Value
Height	2 mm
Length	20 mm
Width	10 mm
Remanence flux density	1.32–1.37 T
Coercity	860–995 $\frac{\text{kA}}{\text{m}}$
Relative permeability	1.056–1.26
Conductivity	5882–9090.9 $\frac{\text{S}}{\text{m}}$

The force acting on the beam is therefore smaller while it moves away from the equilibrium position than when it moves towards it. This slows the oscillation down resulting in an increased damping. However the force is not linearly dependent on the velocity of the beam. This distorts the oscillation behavior of the beam slightly.

2.2.2 Mathematical Description of the System

The system consists of two domains: the mechanical structural dynamics of the beam and the magnetic field. It is therefore necessary to use a coupled model of these two physics to describe it completely [6]. The mechanical system can be described as a second order system

$$\rho \ddot{u}_i + \frac{\partial \sigma_{ij}}{\partial x_j} + f_{i,ext} = 0 \tag{2.1}$$

where σ denotes the stress tensor and f_{ext} the external force. The magnetic field can be described by the magnetic vector potential $\mathbf{A}$

$$\nabla \times \frac{1}{\mu} \nabla \times \mathbf{A} = -\gamma \frac{\partial \mathbf{A}}{\partial t} + \frac{1}{\mu} \nabla \times \mathbf{B}_r \tag{2.2}$$

where μ represents the permeability of the material, $\mathbf{B}_r$ the remanence flux density of the magnets and γ the conductivity of the material.

Both parts of the system can store energy. Assuming a conservative system the energy between the mechanical system and the magnetic domain can be exchanged in both directions. The total energy in the system can therefore be calculated by

$$W = W_{mech} + W_{mag} = W_{kin} + W_{pot} + W_{mag}$$

This can be seen as a potential energy for small displacements (the magnetic potential is not defined for all points in the domain due to singularities at corners. However as long as the integration path does not encircle such a singularity the energy is conservative.) As stated in [5] the change of the magnetic field energy can be described by

$$\mathrm{d}W_{mag} = i\,\mathrm{d}\lambda + f_{mag}\mathrm{d}u \tag{2.3}$$

where λ is the flux linkage, i the currents in any eventual coils, f_{mag} the magnetic force and u the displacement. In this system however we can ignore the first term on the right hand side as there are no coils present. Extending this kind of analysis to the whole system it can be concluded that the only ways of energy entering or leaving the system is by means of external forces f_{ext}, coils, mechanical friction and ohmic losses.

$$d\,W = d \cdot \dot{u} + \gamma \cdot i_{eddy} + i_{coil}\mathrm{d}\lambda + f_{ext} \cdot \mathrm{d}u \tag{2.4}$$

the above mentioned energy exchange by force $f_{mag} \cdot \mathrm{d}u$ becomes in this case an internal energy conversion from the magnetic domain to the mechanical domain and vis versa. It can be seen from (2.3) the magnetic force can be calculated using the principle of virtual work

$$f_{mag} = \frac{\partial W_{mag}}{\partial \mathbf{u}} \tag{2.5}$$

2.2.3 Parameter Identification

In order to determine the magnet properties of the steal used for beam and yoke impedance measurements were conducted. The permeability of metals depends on the manufacturing process. Therefore it is hard to predict this property beforehand. However, this property can be determined by measuring the impedance of a coil winded around the beam or the yoke. This property depends mainly on the conductivity of the material and the permeability. For structural steal that is used in this case the conductivity is roughly known. Therefore the impedance can be used to approximate the permeability.

By simulating the same system in a 3D FEM program the permeability of the material can be estimated. Figure 2.2 shows the comparison between the measured values for the inductance and resistance and the calculated values for different permeabilities and conductivities of the iron material. The instrument used was lacking the capability to measure below a frequency of 20 Hz. It is presumed that due to the skin effect in the iron the inductance drops rapidly for some frequencies

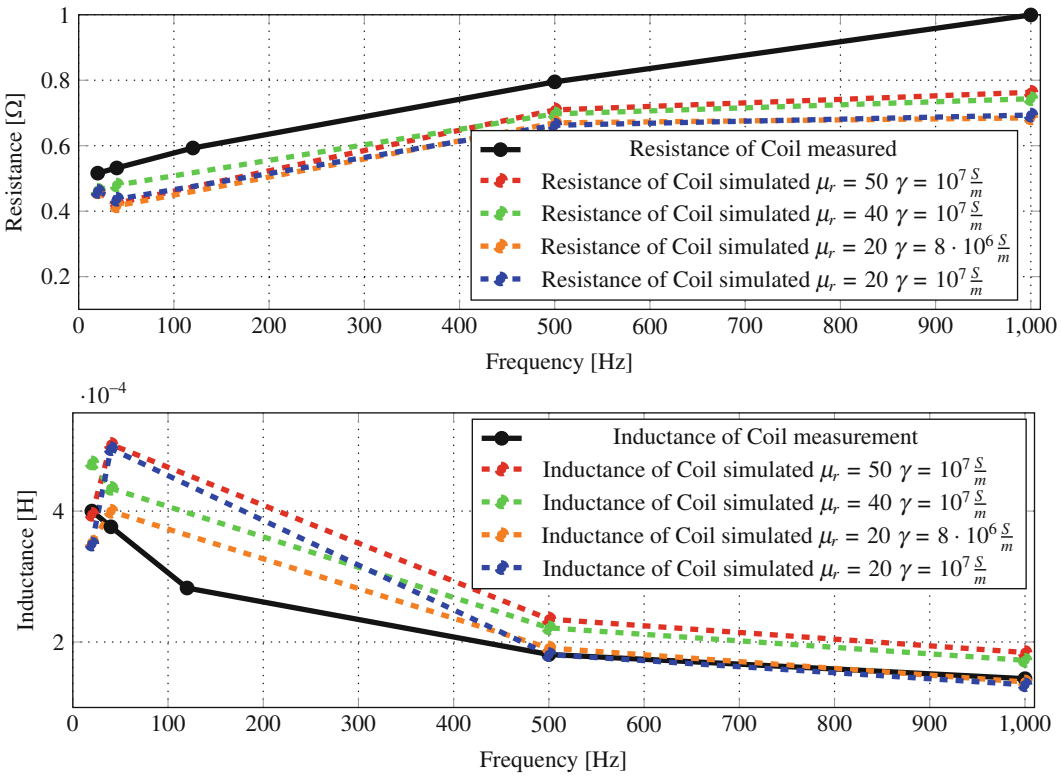

Fig. 2.2 Impedance measurements of the stator yoke

below 20 Hz. Being able to measure this drop at very low frequencies would increase the impact of different permeability and conductivity values on the inductance leading to a more accurate determination of the material properties. At the frequencies measured it can be seen in Figs. 2.3 and 2.2 that the variation of the values has little effect on the inductance making a property identification difficult.

It should also be noted that the devices used has a higher accuracy at higher frequencies. At 20 Hz the error is around 1% of the measured. Therefore it is more important to properly fit the measured data to the simulated one at higher frequencies (Table 2.2).

2.3 3D FEM Model

Above it was discussed that the oscillation are not linear oscillation but slightly distorted. However, in the computer model the assumption is made that the coupled system oscillates linearly around the equilibrium position.

In order to calculate the eigenparameters of this model a monolithic formulation is necessary as it has been done in [3], in [10] for electro-mechanical coupling and in [1] for piezo elements. A 3D analysis of the magnetic field is necessary because the change in magnetic field density can only be predicted accurately by taking the fringe effects around the edges of the magnets and the beam into account. A 2D model would neglect parts of the edges of the system and hence also part of the fringe effects. As a result the calculated change of magnetic force density due to the movement of the geometry that depends on the magnetic flux density would also be underestimated in a 2D model. This would lead to an underestimation of the effect of interest too.

The FEM formulation for the uncoupled system can be looked up in literature [6, 15]. The derivation can be started from the energy of the system and by derivation with respect to the dofs $\mathbf{q}_u$ the stiffness and mass matrices for the uncoupled system can be derived. The continuous function $\mathbf{A}(\mathbf{x})$ and $\mathbf{u}(\mathbf{x})$ are approximated by the shape functions $\mathbf{N}(\mathbf{x})$ and the degrees of freedom $\mathbf{q} = [\mathbf{q}_u \mathbf{q}_A]$ of the discrete system.

$$\mathbf{u} = \mathbf{N}(\mathbf{x}) \cdot \mathbf{q}_u$$

$$\mathbf{A} = \mathbf{N}(\mathbf{x}) \cdot \mathbf{q}_A$$

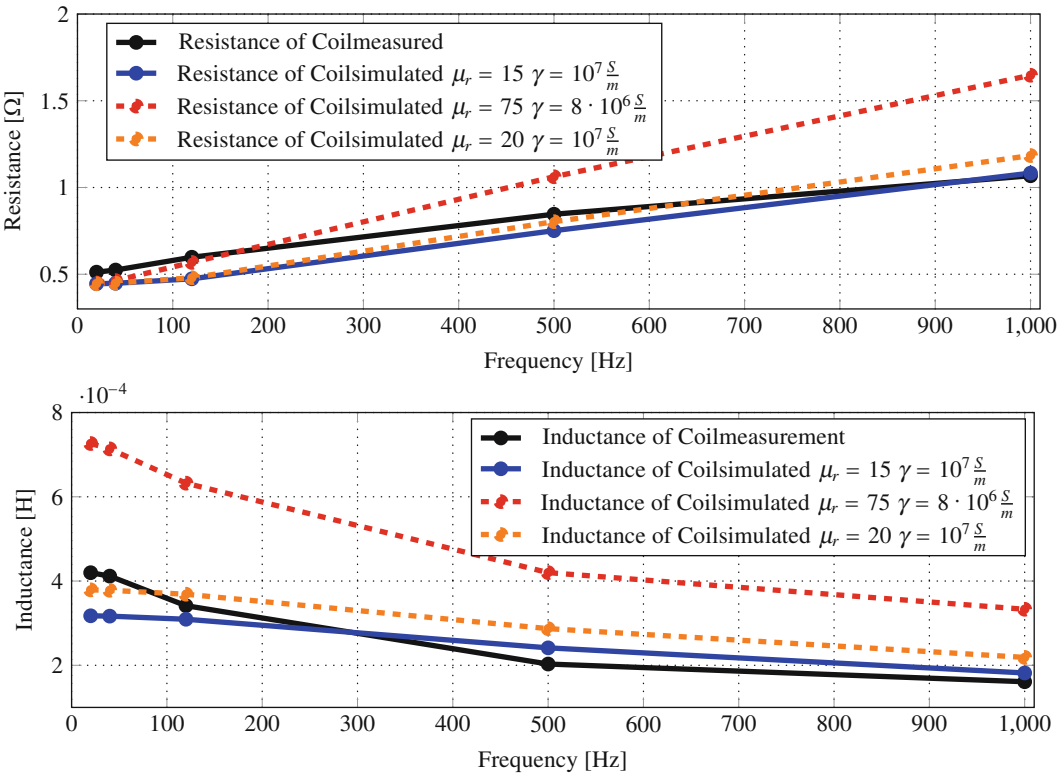

Fig. 2.3 Impedance measurements of the beam

Table 2.2 Chosen parameters for the models

Property	Value
Remanence flux density	1.32 T
Relative permeability	1.06
Conductivity	$0.6 \cdot 10^6 \frac{S}{m}$
Relative permitivity	$1 \frac{F}{m}$
Properties of stator-yoke	
Conductivity	$10^7 \frac{S}{m}$
Relative permitivity	$1 \frac{F}{m}$
Relative permeability	20
Properties of beam	
Conductivity	$10^7 \frac{S}{m}$
Relative permitivity	$1 \frac{F}{m}$
Relative permeability	20
Mass matrix Rayleig damping coefficient	40
Stiffness matrix Rayleig damping coefficient	$6 \cdot 10^{-6}$

Applying these approximations to the energies we can derive the matrices for the discrete system.

$$\mathbf{K}_{uu} = \frac{\partial^2 W_{pot}}{\partial \mathbf{q}_u^2} = \frac{\partial^2}{\partial \mathbf{q}_u^2} \frac{1}{2} \int_\Omega \mathbf{u}^T \mathbf{C} \mathbf{u} \mathrm{d}\Omega \tag{2.6}$$

with $\mathbf{C}$ being the material stiffness matrix which is constant assuming a linear elastic material and a first order finite element.

The Mass matrix can be calculated by taking the second derivative of the kinetic energy with respect to the acceleration of the displacement

$$\mathbf{M}_u = \frac{\partial^2 W_{kin}}{\partial \dot{\mathbf{q}}_u^2} = \frac{\partial^2}{\partial \dot{\mathbf{q}}_u^2} \frac{1}{2} \int_\Omega \dot{\mathbf{u}}^T \rho \dot{\mathbf{u}} \mathrm{d}\Omega \tag{2.7}$$

Rayleigh damping was used to approximate the damping behavior of the beam. The coefficients of the Rayleigh damping α and β were determined by measuring the damping ratio of the system without any interaction with the magnetic field. It was assumed that the damping ratio is the same for 417 Hz and 370 Hz. The Rayleigh damping coefficients were tuned in a 3D FEM model without any magnetic coupling until the measured damping ratio for the two frequencies was reached.

$$\mathbf{D}_u = \alpha \mathbf{M}_u + \beta \mathbf{K}_{uu} \tag{2.8}$$

The magnetic stiffness matrix was calculated in the same way as the mechanical stiffness matrix. Instead of the potential energy the magnetic energy was used.

$$\mathbf{K}_{AA} = \frac{\partial^2 W_{mag}}{\partial \mathbf{q}_A^2} \int_\Omega (\nabla \times \mathbf{A})^T \frac{1}{\mu} (\nabla \times \mathbf{A}) \mathrm{d}\Omega \tag{2.9}$$

the magnetic mass matrix $\mathbf{M}_A$ can be calculated out of the source term $\gamma \frac{\partial \mathbf{A}}{\partial t}$ using the Galerkin method.

$$\mathbf{M}_A = \frac{\partial^2}{\partial \mathbf{q}_A \partial \dot{\mathbf{q}}_A} \int_\Omega \mathbf{A}^T \gamma \dot{\mathbf{A}} \mathrm{d}\Omega \tag{2.10}$$

For the calculation of the magnetic force vector $\mathbf{F}_{mag}$ the Maxwell stress tensor T was used [11,12,14]. This tensor is derived from the principle of virtual work that can be derived from (2.3). It can be shown analog to [10] that the magnetic force can be calculated by

$$\mathbf{F}_{mag} = \frac{\partial}{\partial \mathbf{q}_u} \int_\Omega (\nabla \times \mathbf{A})^T \frac{1}{\mu} (\nabla \times \mathbf{A}) \mathrm{d}\Omega \tag{2.11}$$

The magnetic force represents the first coupling (in this case from the magnetic domain to the mechanical domain). Due to the distortion of the domain caused by the displacement $\mathbf{u}$ the magnetic stiffness and mass matrix as well as the magnetic force vector depend on the displacement $\mathbf{u}$. For the magnetic stiffness and mass matrix this dependency is crucial because this dependency will cause a coupling between the mechanical displacement and the magnetic field.

With these matrices we can formulate the non linear set of equations that describe the coupled system.

$$\begin{aligned} \mathbf{M}_{uu} \cdot \ddot{\mathbf{q}}_u + \mathbf{D}_{\mathbf{uu}} \cdot \dot{\mathbf{q}}_u + \mathbf{K}_{uu} \cdot \mathbf{q}_u &= \mathbf{F}_{ext} + \mathbf{F}_{mag}(\mathbf{q}_u, \mathbf{q}_A) \\ \mathbf{M}_{\mathbf{A}}(\mathbf{q}_u) \cdot \dot{\mathbf{q}}_A + \mathbf{K}_{\mathbf{AA}}(\mathbf{q}_u) \cdot \mathbf{q}_A &= \mathbf{J}_{ext} + \frac{1}{\mu}(\nabla \times \mathbf{B}_r) \end{aligned} \tag{2.12}$$

Each physics for themselves is linear. Coupling the two physical domains will cause the complete set of PDEs to become non linear. Therefore in order to do a modal analysis they need to be linearized. As the oscillation of interest is around the undeformed configuration of the structure and the static magnetic field generated by the permanent magnets, the linearization point is given by those to states.

For such a linearization point (2.12) can be transformed into a linear monolithic system of equations:

$$\underbrace{\begin{bmatrix} \mathbf{M}_u & 0 \\ 0 & 0 \end{bmatrix}}_{\mathbf{M}} \begin{bmatrix} \ddot{\mathbf{q}}_u \\ \ddot{\mathbf{q}}_A \end{bmatrix} + \underbrace{\begin{bmatrix} \mathbf{D}_u & 0 \\ 0 & \mathbf{M}_A \end{bmatrix}}_{\mathbf{D}} \begin{bmatrix} \dot{\mathbf{q}}_u \\ \dot{\mathbf{q}}_A \end{bmatrix} + \underbrace{\begin{bmatrix} \mathbf{K}_{uu} & \mathbf{K}_{uA} \\ \mathbf{K}_{Au} & \mathbf{K}_{AA} \end{bmatrix}}_{\mathbf{K}} \underbrace{\begin{bmatrix} \mathbf{q}_u \\ \mathbf{q}_A \end{bmatrix}}_{\mathbf{q}} = \underbrace{\begin{bmatrix} \mathbf{F}_{ext} \\ \mathbf{J}_{ext} + \mathbf{L}_{PM} \end{bmatrix}}_{\mathbf{L}} \tag{2.13}$$

The coupling matrices $\mathbf{K}_{uA}$ and $\mathbf{K}_{Au}$ can be derived from the magnetic force and therefore from the energy stored in the magnetic field.

$$\mathbf{K}_{uA} = \frac{\partial \mathbf{F}_{mag}}{\partial \mathbf{q}_A} = \frac{\partial}{\partial \mathbf{q}_A} \left(\frac{\partial}{\partial \mathbf{q}_u} W_{mag} \right) = \frac{\partial}{\partial \mathbf{q}_u} \left(\frac{\partial}{\partial \mathbf{q}_A} W_{mag} \right) = \frac{\partial}{\partial \mathbf{q}_u} (\mathbf{J}_{int}) = \mathbf{K}_{Au} \tag{2.14}$$

Looking at Eq. (2.14) it can be assumed that the total stiffness matrix is symmetric. However, in the FEM code used for the simulation the stiffness coupling matrix $\mathbf{K}_{uA}$ is derived in another way which ruins this symmetry.

Using the Maxwell stress tensor $\mathbf{T}$ the specific magnetic force acting on a structure can be computed by

$$\mathbf{f}_{mag} = \nabla \cdot \mathbf{T} = \nabla \cdot \left(\mathbf{H}\mathbf{B}^T - \mathbf{I} \frac{\mathbf{H} \cdot \mathbf{B}}{\mu} \right) \tag{2.15}$$

where $\mathbf{I}$ denotes the identity matrix. The force acting on a whole domain can therefore be represented by the integral of the specific force on that domain

$$\mathbf{F}_{mag} = \int_{\Omega} \mathbf{f}_{mag} \mathrm{d}\Omega = \int_{\Omega} \nabla \cdot \mathbf{T} \mathrm{d}\Omega \tag{2.16}$$

Using the divergence theorem we can write this integral as an integral over the surface of the domain $\partial\Omega$

$$\mathbf{F}_{mag} = \int_{\partial\Omega} \mathbf{n} \cdot \mathbf{T}(\mathbf{A}) \mathrm{d}\partial\Omega \tag{2.17}$$

where $\mathbf{n}$ is the normal vector pointing outwards of the domain boundary. For a domain where the gradient of the magnetic field throughout the domain is almost zero the magnetic forces created within the domain are negligible. This is an assumption that holds for iron because the permeability of that iron is so high that the resulting gradients of the magnetic field are small compared to the gradients at its surface. In that case only the forces on the surface of the domain contribute to the total magnetic force. Therefore the projection of the magnetic forces from within the domain on its surface is negligible and therefore the therm $\mathbf{n} \cdot \mathbf{T}$ actually represents the local stress on the surface of the domain.

Starting the derivation of the stiffness matrix with (2.17) yields a different matrix than the derivation starting with (2.11). The same result has been discovered in [13] for electro-static field forces.

Starting from (2.17) we can the derive the coupling matrix $\mathbf{K}_{uA}$

$$\mathbf{K}_{uA} = \frac{\partial}{\partial \mathbf{q}_A} \int_{\partial\Omega} \mathbf{n} \cdot \mathbf{T}(\mathbf{A}) \mathrm{d}\partial\Omega \tag{2.18}$$

The matrices formulated in (2.13) can be rewritten in the quadratic eigenvalue problem:

$$\left(\mathbf{K} + j \cdot \lambda_r \mathbf{D} - \lambda_r^2 \mathbf{M}\right) \mathbf{q}_r = 0 \tag{2.19}$$

where $\mathbf{q}_r$ represent the eigenvector and λ_r the eigenvalues. Solving this eigenvalue problem yields the modes and resonance frequencies of the coupled system.

2.4 Measurements

Using a laser doppler vibrometer (LDV) hammering tests where conducted to measure the frequency and damping behavior of the first bending mode of the beam. These measurements where done in three different positions of the beam: completely out of the air gap, completely inserted in the air gap and half way inserted in the air gap. The modal parameters where evaluated by fitting a decaying sinusoidal function to the data using a least square evaluation.

$$\underset{y_0,\, \omega_n,\, \zeta}{\text{minimize}} \left(\sum_t (x(t) - y(t - t_0))^2 \right) \quad \text{for } t \in [t_0, t_0 + \Delta t] \tag{2.20}$$

$$\text{with} \quad y(t) = y_0 \cdot e^{-2\pi\, \omega_n\, (\zeta + \sqrt{\zeta^2 - 1})}$$

where ζ, ω_n and y_0 are the parameters to identify. I is the cost function and $x(t)$ the measurement data. The measured data $x(t)$ and the decaying sinusoidal function $y(t)$ are aligned by setting $x(t_0) = max(x(t))$ and choosing an arbitrary length Δt. The measured parameters are shown in Table 2.3.

Table 2.3 Simulation results and measurements

	3d-Model		Measurement	
	Frequency	Damping	Frequency	Damping
No EM coupling	417.1 Hz	$\zeta = 1.66\%$	417 Hz	$\zeta = 1.66\%$
With EM coupling	371.7 Hz	$\zeta = 3.32\%$	370 Hz	$\zeta = 3.6\%$
Half EM coupling	387.1 Hz	$\zeta = 2.62\%$	384.6 Hz	$\zeta = 2.25\%$

2.5 Results

The measurements show clearly a trend towards more damping and a lower system in the system than before. Table 2.3 shows the simulated and measured eigenfrequencies and damping ratios of the system. For the case where the beam is completely inserted in the air gap, the frequency change is over estimated by the 3D model while the damping is underestimated. Considering that the system introduced is not linear the expected agreement with the linear 3D model cannot be perfect. It was shown that it is possible to do a approximation using the linearized set of equations and a linear modal analysis.

2.6 Conclusion and Outlook

A monolithic eigenvalue formulation for magneto-mechanical coupled problems was introduced. It could be shown that a 3D FEM model using this formulation can predict the eigenbehavior of magneto-mechanical coupled systems. Although the measured data deviates slightly from the simulated data it is clear that the effects of interest are qualitatively correctly predicted by the model.

In future research the demonstrated methods will be applied to wind turbine generators in order to allow a coupled modal analysis of the system and to analyze to what extend the structural dynamics are influenced by the magnetic field.

References

1. Allik H, Hughes TJR (1970) Finite element method for piezoelectric vibration. Int J Numer Meth Eng 2(2):151–157
2. Belahcen A (2005) Magnetoelastic coupling in rotating electrical machines. IEEE Trans Magn 41(5):1624–1627
3. Belahcen A (2006) Vibrations of rotating electrical machines due to magnetomechanical coupling and magnetostriction. IEEE Trans Magn 42(4):971–974
4. Furlan M, Cernigoj A, Boltezar M (2003) A coupled electromagnetic-mechanical-acoustic model of a DC electric motor. COMPEL: Int J Comput Math Electr Electron Eng 22(4):1155–1165
5. Herbert Woodson JRM (1968) Electromechanical dynamics. Wiley, New York
6. Kaltenbacher M (2007) Numerical simulation of mechatronic sensors and actuators. Springer, New York
7. Maxwel JC (1865) A dynamical theory of the electromagnetic field
8. Pellerey P, Lanfranchi V, Friedrich G (2012a) Coupled numerical simulation between electromagnetic and structural models. Influence of the supply harmonics for synchronous machine vibrations. IEEE Trans Magn 48(2):983–986
9. Pellerey P, Lanfranchi V, Friedrich G (2012b) Coupled numerical simulation between electromagnetic and structural models. Influence of the supply harmonics for synchronous machine vibrations. IEEE Trans Magn 48(2):983–986
10. Rochus V, Rixen DJ, Golinval J-C (2006) Monolithic modelling of electro-mechanical coupling in micro-structures. Int J Numer Method Eng 65(4):461–493
11. Sanchez-Grandia R, Vives-Fos R, Aucejo-Galindo V (2006) Magnetostatic Maxwell's tensors in magnetic media applying virtual works method from either energy or co-energy. Eur Phys J Appl Phys 35(01):61–68
12. Sanchez Grandia R, Aucejo Galindo V, Usieto Galve A, Vives Fos R (2008) General formulation for magnetic forces in linear materials and permanent magnets. IEEE Trans Magn 44(9):2134–2140
13. Stephan H (2010) Modeling strategies for electro - mechanical microsystems with uncertainty quantification door. PhD thesis
14. Vandevelde L (2001) A survey of magnetic force distributions based on different magnetization models and on the virtual work principle. IEEE Trans Magn 37(5):3405–3409
15. Zienkiewicz OC, Taylor RL, Zhu JZ (2005) The finite element method: its basis and fundamentals, vol 1 of The finite element method. Elsevier Butterworth-Heinemann

http://www.springer.com/978-3-319-04773-7

Topics in Modal Analysis II, Volume 8
Proceedings of the 32nd IMAC, A Conference and Exposition on Structural Dynamics, 2014
Allemang, R. (Ed.)
2014, IX, 416 p. 413 illus., 352 illus. in color., Hardcover
ISBN: 978-3-319-04773-7